Journal Pre-proofs

Event-triggered robust model reference adaptive control for drag-free satellite

Xiao-yun Sun, Qiang Shen, Shu-fan Wu

PII:	S0273-1177(23)00746-9
DOI:	https://doi.org/10.1016/j.asr.2023.09.024
Reference:	JASR 16968
To appear in:	*Advances in Space Research*
Received Date:	10 November 2022
Accepted Date:	11 September 2023

Please cite this article as: Sun, X-y., Shen, Q., Wu, S-f., Event-triggered robust model reference adaptive control for drag-free satellite, *Advances in Space Research* (2023), doi: https://doi.org/10.1016/j.asr.2023.09.024

Available online at www.sciencedirect.com

ScienceDirect

Advances in Space Research xx (2023) xxx-xxx

ADVANCES IN SPACE RESEARCH
(a COSPAR publication)

www.elsevier.com/locate/asr

Event-triggered robust model reference adaptive control for drag-free satellite

Xiao-yun Sun[a,b], Qiang Shen[a,b], Shu-fan Wu[a,b,*]

[a]School of Aeronautics and Astronautics, Shanghai Jiaotong University, Shanghai 200240, China
[b]Shanghai Frontier Science Center for Gravitational Wave Detection, Shanghai 200240, China

Abstract

Aiming at the requirement of bounded disturbance suppression for low-frequency space gravitational wave detection satellite, a robust model reference adaptive drag-free control scheme is proposed in this paper via linear matrix inequalities (LMIs) approach. The multivariable model reference adaptive control (MRAC) scheme is applied to the drag-free control system with parameter uncertainties, which realizes the adaptive tracking to the reference state. The LMI system is established as an adaptive compensation term, which provides robustness against nonlinear disturbances. To reduce the communication burden of the actuation information and further save the total energies, an event-triggered mechanism (ETM) is introduced, with both the actuation inputs and the adaptive laws of the feedback gains updated only at the triggering time instants. The ultimately uniformly boundedness of the closed-loop signals is proved by Lyapunov analysis, with each system state convergence. From the feasibility analysis, Zeno behavior can be further proved to be strictly excluded. The numerical simulation verifies that the proposed scheme has efficient robustness to nonlinear disturbances with low energy cost, and achieves good effect in response to the requirements of space gravitational wave detection mission.

Keywords: Space gravitational wave detection; Drag-free control; Linear matrix inequality; Event triggered mechanism ; Model reference adaptive control

1. Introduction

In a mission of space gravitational wave detection, the detection spacecraft is required to have strong robustness to ensure the successful detection of low-frequency gravitational wave signals (Fichter et al., 2005). Drag-free control is a main scheme applied for the spacecraft platform with the internal test masses (TMs) (Mobley et al., 1975). The TMs in the detection spacecraft are utilized as the key payload to provide an inertial reference for the spacecraft's on-orbit motion and to achieve ultra-high precision and accurate tracking of the spacecraft attitude dynamics (Fichter et al., 2007).

A typical example of the mission is the low-frequency space gravitational wave detection mission (Luisella et al., 2013). In the millihertz frequency band, the desired residual perturbation acceleration of the sensitive axis is better than the order of $10^{-15} m/s^2/\sqrt{Hz}$, and the displacement control accuracy of the spacecraft is better than the order of $1nm/\sqrt{Hz}$ (Enrico et al., 2009; Wu & et al., 2011). These desired performance indexes provide necessary technical support for the generation of next space gravitational wave detection projects (Enrico., 2008). However, these performance requirements are extremely challenging for the design of the control scheme due to the existence of system uncertainties and disturbances for near-Earth satellites (Wu & et al., 2010).

Various drag-free control schemes and satellite attitude control schemes are developed to deal with those uncertainties and disturbances such as nonlinear control schemes (Shen et al., 2018; Shen & et al., 2020; Li et al., 2019, 2017; Gui., 2021)

*Corresponding author: Tel.: +86-158-0053-7342
Email addresses: sunxiaoyun@sjtu.edu.cn (Xiao-yun Sun), qiangshen@sjtu.edu.cn (Qiang Shen), Shufan.wu@sjtu.edu.cn (Shu-fan Wu)

https://dx.doi.org/10.1016/j.jasr.xxxx.xx.xxx

and linear control schemes (Wu & Fertin., 2008; Lian & et al., 2021). In nonlinear control schemes, system uncertainties and disturbances are often estimated and suppressed by the model approximation or prediction capability, such as adaptive control (Shen et al., 2018; Shen & et al., 2020; Li et al., 2019, 2017) and sliding mode control (Gui., 2021). In linear control schemes, controllers are designed based on approximate small-disturbance linearization dynamics. In Wu & Fertin. (2008), a controller is designed based on quantitative feedback theory (QFT) in the decoupled drag-free control loop. In Lian & et al. (2021), a hybrid sensitivity H_∞ control scheme based on a frequency separation strategy is proposed, which can meet the drag-free control requirements under measurement constraints in Scientific Mode.

Event-triggered control (ETC) has been recently suggested as an alternative to conventional periodic sampling control due to its distinctive advantages. The key idea of ETC is that the control update is not performed as long as the performance of the closed-loop system is satisfactory, unlike conventional periodic sampling control where the sampling period is determined by considering the worst scenario, and thus many unnecessary samplings have to be carried out (Liu et al., 2020; Wang et al., 2018; Qiu et al., 2019; Wang et al., 2022; Xing & et al., 2016; Zhang & Yang., 2018; Liang & et al., 2020; Long & Wang., 2021). In the field of satellite control, event-triggered control would be able to reduce the communication burden and save the energy consumption of payloads and actuators with satisfactory performance (Wang & Chen., 2020; Qian et al., 2021; Zhang & et al., 2021). A distributed event-triggered adaptive control law is proposed to study the consensus of a group of multiple uncertain rigid spacecraft systems in Liu et al. (2020), and an event-triggered observer is designed to solve the formation tracking control problem of multiple spacecraft systems limited by communication resources in Wang et al. (2018).

Motivated by the above discussions, a novel event-triggered robust model reference adaptive control (ETRMRAC) scheme is developed for the drag-free satellite in the mission of low-frequency space gravitational wave detection. The major contributions of this paper in comparison to those existing works are summarized as follows.

Firstly, an enhanced robust model reference adaptive control (MRAC) method is proposed combining with the linear matrix inequalities (LMIs) and firstly applied to a drag-free control system. Compared with the aforementioned robust control scheme for the drag-free system (Wu & Fertin., 2008; Lian & et al., 2021), the nonlinearities are concerned through the compensator modified by the LMI approach, and the closed-loop signals can adaptively track the reference model. The LMIs are introduced to drive the Lyapunov candidate function so that each closed-loop signal can converge to a bound.

Secondly, a novel event-triggered mechanism (ETM) is designed for the LMI-based MRAC scheme, which can guarantee the robustness of the sensitive axis response while strictly avoiding the Zeno behavior. The controller is updated only at each triggering time, which can deal with nonlinear external disturbances with low actuation and communication costs. Compared with the event-triggered approach reported in (Wang et al., 2018; Qiu et al., 2019; Wang et al., 2022), extra robustness is provided to behave effective performance when there exists parameter uncertainties and state-related disturbances.

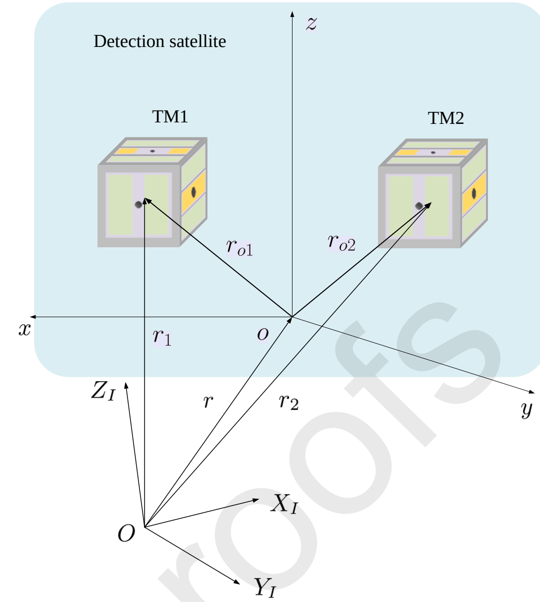

Fig. 1. The multi-body configuration of the TMs and the detection satellite.

The rest of the paper is organized as follows: in Section II, the dynamic model and control framework is formulated, which establishes the nonlinear dynamics of the drag-free satellites with 6 degrees of freedom (DOFs) sensitive axis. In Section III, the ETRMRAC scheme is designed, with the design of ETM according to tracking errors, the LMIs are constructed by the adaptive control synthesis, and the ultimate boundedness of the closed-loop signal is analyzed based on the Lyapunov method. In Section IV, numerical simulation is carried out to verify the efficiency of the scheme, Section V gets the conclusion.

2. Problem Formulation

In this section, the multibody drag-free control dynamic model of the proposed system is established, and the control framework and the assumptions required are established.

2.1. Modeling of Drag-free Control Systems

Take the LISA Pathfinder gravitational wave detection mission as an example (McNamara & et al., 2008; Zanoni & Bortoluzzi., 2015; Grynagier et al., 2013; Ziegler et al., 2014) to model the dynamics of the drag-free control system. The satellite consists of two opposing inertial TMs named TM1 and TM2, and the multi-body configuration of the TMs and the detection satellite is given in Fig. 1. As shown in Fig. 1, $o - xyz$ denotes the body frame of the detection satellite, and $O{-}X_IY_IZ_I$ is the inertia frame. r, r_1, r_2 are the absolute motion of the satellite and the TMs, r_{o1}, r_{o2} represent the relative motion between the satellite and the TMs. According to the analysis in Grynagier et al. (2013), the multi-body dynamics equation can be described as the following approximate second-order form:

$$M_q \ddot{q}^* = K_{LTP} q^* + K_h q + f_{stray} + f_{actuation} + M_u \ddot{u}_{SC}, \tag{1}$$

where, $f_{actuation}$ is the nominal force of the low-frequency suspension, f_{stray} is the total force or moment noise including various sources. K_{LTP} is the internal stiffness of the multi-body systems, K_h is the parasitic stiffness of the inertial sensor, q^* is the satellite displacement relative to the mechanical deformation of each TM with the consideration of housing and optical table of n_{LTP} and the mechanical deformation n_{SC}, q is the nominal displacement of TM relative to the satellite, M_q, M_u are the mass matrix and sensitivity matrix relative to the absolute satellite motion, $\ddot{u}_{SC}$ is the absolute motion of the satellite.

Express the absolute motion of the satellite and the TMs as:

$$q = \left[r_1^{\mathrm{T}}, \varphi_1^{\mathrm{T}}, r_2^{\mathrm{T}}, \varphi_2^{\mathrm{T}}\right]^{\mathrm{T}}, u_{SC} = \left[r^{\mathrm{T}}, \varphi_{SC}^{\mathrm{T}}\right]^{\mathrm{T}},$$

where $r = [x_{SC}, y_{SC}, z_{SC}], \varphi_{SC} = [\theta_{SC}, \eta_{SC}, \psi_{SC}], r_i = [x_i, y_i, z_i], \varphi_i = [\theta_i, \eta_i, \psi_i], i = 1, 2$. Considering a detailed representation of the sensitivity matrix expressed based on the nominal position vector, the mass and the inertia moment of the TMs are given as:

$$M_q = \begin{bmatrix} m_1 E & 0 & 0 & 0 \\ 0 & I_1 & 0 & 0 \\ 0 & 0 & m_2 E & 0 \\ 0 & 0 & 0 & I_2 \end{bmatrix}, M_u = \begin{bmatrix} -m_1 E & m_1 \tilde{r}_{o1} \\ 0 & -I_1 \\ -m_2 E & m_2 \tilde{r}_{o2} \\ 0 & -I_2 \end{bmatrix},$$

where, E is the identity matrix, m_1, m_2, I_1, I_2 are the TM mass and inertia moment, $\tilde{r}_{o1}, \tilde{r}_{o2}$ are the obliquely symmetric crossover matrix defined by the nominal relative position vector $r_{o1} = \left[r_{o1,x}, r_{o1,y}, r_{o1,z}\right]^{\mathrm{T}}, r_{o2} = \left[r_{o2,x}, r_{o2,y}, r_{o2,z}\right]^{\mathrm{T}}$, expressed as

$$\tilde{r}_{o1} = \begin{bmatrix} 0 & -r_{O1,z} & r_{O1,y} \\ r_{O1,z} & 0 & -r_{O1,x} \\ -r_{O1,y} & r_{O1,x} & 0 \end{bmatrix}, \tilde{r}_{o2} = \begin{bmatrix} 0 & -r_{O2,z} & r_{O2,y} \\ r_{O2,z} & 0 & -r_{O2,x} \\ -r_{O2,y} & r_{O2,x} & 0 \end{bmatrix}.$$

Considering $q^* = q$, and assuming that there are only small-angle rotations in the system dynamics, a further simplified form is given:

$$\begin{bmatrix} I_{SC} & 0 & 0 & 0 & 0 \\ -m_1 T_{1B} \tilde{r}_{o1} & m_1 E & 0 & 0 & 0 \\ I_1 T_{1B} & 0 & I_1 & 0 & 0 \\ -m_2 T_{2B} \tilde{r}_{o2} & 0 & 0 & m_2 E & 0 \\ I_2 T_{2B} & 0 & 0 & 0 & I_2 \end{bmatrix} \begin{pmatrix} \ddot{\varphi}_{SC} \\ \ddot{r}_1 \\ \ddot{\varphi}_1 \\ \ddot{r}_2 \\ \ddot{\varphi}_2 \end{pmatrix} = \begin{pmatrix} t \\ f_1 - \frac{m_1}{m} T_{1B} f \\ t_1 \\ f_2 - \frac{m_2}{m} T_{2B} f \\ t_2 \end{pmatrix}, \tag{2}$$

where T_{1B}, T_{2B} are the transformation matrices from the satellite main body to the TMs at the nominal position. Define the accelerations of the satellite and TMs as:

$$\alpha = I^{-1} t, a = \frac{1}{m} f, \alpha_1 = I_1^{-1} t_1,$$
$$a_1 = \frac{1}{m_1} f_1, \alpha_2 = I_2^{-1} t_2, a_2 = \frac{1}{m_2} f_2,$$

where $m_1, m_1, m_2, I, I_1, I_2$ are the mass and inertia moment of the spacecraft and TMs respectively.

According to the rules of the LISA Pathfinder mission, when executing Scientific Mode 1 (or Test Mode M3), 3-DOF of translational, 1-DOF of rotational in TM1, and 2-DOFs of rotational in TM2 are selected to realize drag-free control, with the other 6-DOF for electrostatic suspension control (Ziegler et al., 2014). According to the coordinate selection matrix D_{DF}, D_{SUS} given in Li et al. (2019), the drag-free system dynamics are reformulated as:

$$\begin{pmatrix} \ddot{\varphi}_{SC} \\ \ddot{q}_{DF} \\ \ddot{q}_{SUS} \end{pmatrix} = \begin{bmatrix} B_{ATT} & 0 \\ D_{DF} B_1 & D_{DF} B_2 \\ D_{SUS} B_1 & D_{SUS} B_2 \end{bmatrix} \begin{pmatrix} a_{SC} \\ a_{TM} \end{pmatrix}, \tag{3}$$

where, q_{DF}, q_{SUS} are the drag-free control and electrostatic suspension control coordinates, $q_{DF} = D_{DF} q, q_{SUS} = D_{SUS} q, q = \left[r_1^{\mathrm{T}}, \varphi_1^{\mathrm{T}}, r_2^{\mathrm{T}}, \varphi_2^{\mathrm{T}}\right]^{\mathrm{T}}$. B_1, B_2, B_{ATT} are the more compact parameter matrices, which are defined as:

$$B_{ATT} = \begin{bmatrix} 0 & \tilde{x} \end{bmatrix}, B_1 = \begin{bmatrix} -T_{1B} & T_{1B} \tilde{r}_{o1} \\ 0 & -T_{1B} \\ -T_{2B} & T_{2B} \tilde{r}_{o2} \\ 0 & -T_{2B} \end{bmatrix}, B_2 = E,$$

a_{SC}, a_{TM} are the combined external force and torque on the spacecraft and the TMs, $a_{SC} = \begin{pmatrix} a^{\mathrm{T}} & \alpha^{\mathrm{T}} \end{pmatrix}^{\mathrm{T}}, a_{TM} = \begin{pmatrix} a_1^{\mathrm{T}} & \alpha_1^{\mathrm{T}} & a_2^{\mathrm{T}} & \alpha_2^{\mathrm{T}} \end{pmatrix}^{\mathrm{T}}$. Considering that the total external force and torque are input by the controller u_T, u_S, disturbance d_{SC}, d_{TM} and TM stiffness deformation, the system dynamics are finally expressed as:

$$\begin{aligned} \begin{pmatrix} \ddot{\varphi}_{SC} \\ \ddot{q}_{DF} \\ \ddot{q}_{SUS} \end{pmatrix} &= \begin{bmatrix} B_{ATT} & 0 & 0 \\ B_{DF} & E & 0 \\ B_{SUS} & 0 & E \end{bmatrix} \left(\begin{pmatrix} u_T \\ u_{S1} \\ u_{S2} \end{pmatrix} + \begin{pmatrix} d_{SC} \\ d_{TM1} \\ d_{TM2} \end{pmatrix} \right) \\ &+ \begin{bmatrix} 0 & 0 & 0 \\ 0 & -\Omega_{DF}^2 & 0 \\ 0 & -\Omega_C^2 & -\Omega_{SUS}^2 \end{bmatrix} \begin{pmatrix} \varphi_{SC} \\ q_{DF} \\ q_{SUS} \end{pmatrix}, \end{aligned} \tag{4}$$

where, $B_{DF} = D_{DF} B_1, B_{SUS} = D_{SUS} B_1$, $u_{S1} = D_{DF} B_2 u_S, u_{S2} = D_{SUS} B_2 u_S$ are controller inputs, $d_{TM1} = D_{DF} B_2 d_{TM}, d_{TM2} = D_{SUS} B_2 d_{TM}$ are drag-free system input noise. $\Omega_{DF}^2, \Omega_{SUS}^2$ and Ω_C^2 are stiffness matrices, Ω_{DF}^2 and Ω_{SUS}^2 are diagonal matrices. Only analyze the drag-free loop, the state is defined as $x = [q_{DF}, \dot{q}_{DF}]^{\mathrm{T}}$, then the drag-free loop considering input disturbance can be expressed as:

$$\begin{aligned} \dot{x} &= Ax + B(u_T + d_{TM}), \\ y &= Cx, \end{aligned} \tag{5}$$

where, $d_{TM} = B^{-1}(u_{S1} + d_{TM1}) + d_{SC}$ is the total noise, A, B, C are the state parameter matrices, $A = \begin{bmatrix} 0 & E \\ -\Omega_{DF}^2 & 0 \end{bmatrix}, B = \begin{bmatrix} 0 \\ B_{DF} \end{bmatrix}$. Assuming that A, B are slowly time-varying, y is the output. The feedback controller is designed to satisfy the following model matching conditions (Li et al., 2017):

$$\dot{x}_m(t) = A_m x_m + B_m r(t), A_m = A + B k_x^{*\mathrm{T}}, B_m = B k_r^*, \tag{6}$$

where A_m, B_m are the reference model parameter matrices, y_m is the reference output, k_x^*, k_r^* are the nominal feedback gain,

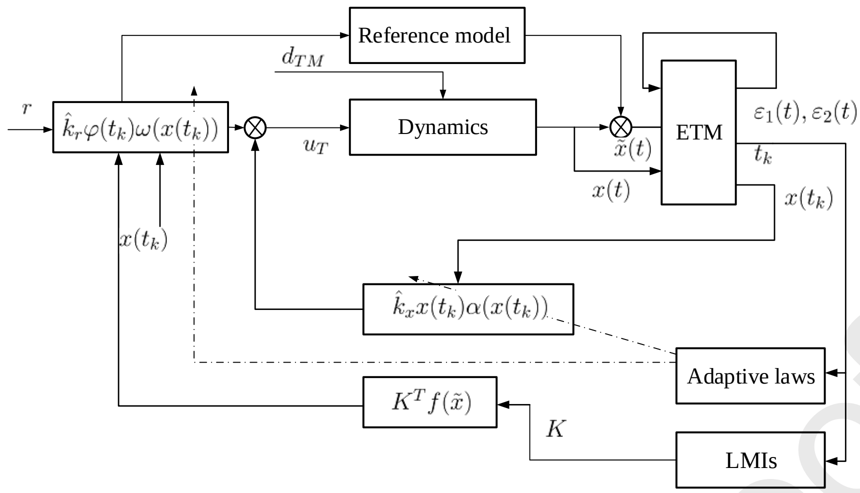

Fig. 2. Control framework.

assuming k_r^* has an upper bound $\bar{k}_r^*$. The following assumptions are given:

Assumption 2.1: The disturbance term $d_{TM}(t)$ is continuous and bounded, which satisfies the following inequality:

$$\|d_{TM}\| \leq \bar{d}_{TM} + L\|\tilde{x}\| + L_1\|\tilde{x}\|^{1+\eta} + L_2\|\tilde{x}\|^{1+\theta}, \tag{7}$$

where $\bar{d}_{TM}, L, L_1, L_2 \in \mathbb{R}_+$ is assumed to be known, the state tracking error $\tilde{x}(t) = x(t) - x_m(t)$, x_m is the reference state, $\eta \in (0,1), \theta > 1$. The assumption of disturbance characteristics is related to the strong nonlinearities of the actual conditions in the space detection missions (Franco et al., 2021).

Assumption 2.2: The chosen of the reference state matrix A_m needs to be mentioned. The control objective of this work is to drive the drag-free system to a stable linear decoupled system, which is similar to the goal in (Wu & Fertin., 2008), so that the closed-loop signals can converge to a bound and the system is stable. The chosen result of A_m can be found in the section of Simulation Results and Analysis, which implies A_m is a diagonal stable matrix.

2.2. Control Framework

The control framework is shown in Fig. 1. Under the premise of precise control in the drag-free system, to realize the approximation and feedback of continuous and bounded additional disturbances, and improve the information transmission efficiency and system robustness, the ETRMRAC framework is established. The feedback correction term based on the LMI approach is modified in the controller design, to enhance the global robustness in the interevent time. The ETM is introduced in the MRAC law of the multi-variable drag-free control system, to guarantee the parameter adaptive laws are only updated at each triggering time instant.

3. Drag-free Control System Design by ETRMRAC

In this section, the ETM is given first, the control law and adaptive law are designed with the LMIs constructed based on the stability analysis, and the global boundedness of each closed-loop signal and Zeno behavior are then analyzed.

3.1. ETM Design

To design the ETM, the closed-loop system is firstly divided into unequally time intervals, and under the k-th time transient t_k with $k \in \mathbb{N}$, an event-triggered parameter adaptation law is carried out, and the control law is updated accordingly. Define the sampling errors as:

$$\varepsilon_1(t) = x(t) - x(t_k), \varepsilon_2(t) = \varphi(t) - \varphi(t_k) \tag{8}$$

where φ is defined in (12). and it is assumed that the first event occurs at $t_0 = 0$. The ETM is to sample the state of the plant (5) at each triggering instant. Without loss of generality, the initial value of the sample time is $t_0 = 0$. The length of time interval between each two consecutive trigger time instants is defined as the interevent time. and the event-triggered transient state is called the instant state (Lu et al., 2019). Define the ETM as:

$$\begin{aligned} t_{k+1} = \inf\{ & t > t_k | \iota(\Phi - \mu L)\|\tilde{x}(t)\|^2 - 8\gamma\|x(t)\|^2 - \|x(t)\|^4 \\ & - \|\varphi(t)\|^4 - 2\gamma\|\varepsilon_1(t)\|^2 - 2\varpi\|\varepsilon_2(t)\|^2 - 8\varpi\|\varphi(t)\|^2 \\ & - \iota(\Phi - \mu L)m_0 \mathrm{e}^{-m_1 t} = 0\}, \end{aligned} \tag{9}$$

where, $m_0 > 0, m_1 > 0$, other parameters to be designed are given by **Theroem 3.1**.

3.2. Controller Design

Substituting (6) into the plant (5) and rewriting the closed-loop system as:

$$\dot{x} = A_m x + B_m k_r^{*-1}\left(u_T + d_{TM} - k_x^{*\mathrm{T}} x\right). \tag{10}$$

The nominal robust state feedback control input $u_T^*(t)$ is given as:

$$u_T^*(t) = k_x^{*\mathrm{T}} x(t) + k_r^* r(t) + k_r^* K^{\mathrm{T}} f(\tilde{x}), \tag{11}$$

where, $f(\tilde{x}) = \left[f_0^{\mathrm{T}}(\tilde{x}), f_1^{\mathrm{T}}(\tilde{x}), f_2^{\mathrm{T}}(\tilde{x})\right]^{\mathrm{T}}$, $f_0(\tilde{x}) = \|\tilde{x}\|^0 sgn(\tilde{x})$, $f_1(\tilde{x}) = \|\tilde{x}\|^\eta sgn(\tilde{x}), f_2(\tilde{x}) = \|\tilde{x}\|^\theta sgn(\tilde{x}), \eta \in (0,1), \theta > 1$, K

is the robust feedback gain. When there are uncertainties in the system state, the nominal feedback gain k_x^*, k_r^* will not be accurately obtained. Let $\varphi(r, \tilde{x}) = r + K^{\mathrm{T}} f(\tilde{x})$, rewrite (9) as

$$\begin{aligned} \dot{x} &= A_m x + B_m r + B_m k_r^{*-1} \\ &\times \left(u_T - k_x^* x - k_r^* \varphi(\tilde{x}, r) + k_r^*\left(\bar{d}_0 + K^{\mathrm{T}} f(\tilde{x})\right)\right), \end{aligned} \tag{12}$$

where $\bar{d}_0 = k_r^{*-1} d_{TM}$, which is obviously bounded and satisfies **Assumption 2.1**. First, under the time interval $[t_k, t_{k+1})$, the interevent controller is applied as:

$$u_T(t) = \hat{k}_x^{\mathrm{T}} x(t_k)\, \alpha(x(t_k)) + \hat{k}_r \varphi(t_k)\, \omega(x(t_k)) \tag{13}$$

where,

$$\begin{aligned} \alpha(x(t_k)) &= \tanh\left(\frac{1}{\epsilon}\hat{k}_x^{\mathrm{T}} x(t_k)\left(\tilde{x}^{\mathrm{T}}(t_k) P + f^{\mathrm{T}}(\tilde{x}(t_k))\Lambda\right) B_m\right), \\ \omega(x(t_k)) &= \tanh\left(\frac{1}{\epsilon}\hat{k}_r \varphi(x(t_k), r)\left(\tilde{x}^{\mathrm{T}}(t_k) P + f^{\mathrm{T}}(\tilde{x}(t_k))\Lambda\right) B_m\right), \end{aligned} \tag{14}$$

$\Lambda = [\Lambda_0, \Lambda_1, \Lambda_2]^{\mathrm{T}}, \Lambda_j = \mathrm{diag}\left\{\lambda_{ji}\right\}, \lambda_{ji} \in \mathbb{R}_+, i = 1, ..., n$, ϵ is a small positive constant, $\epsilon \in \mathbb{R}_+$, $P = P^{\mathrm{T}} \in \mathbb{R}^{n\times n}, P \geq 0$, $\hat{k}_x, \hat{k}_r$ are the parameters to be estimated that are updated only in the triggering time, that is, in the interevent state, the parameter adaptive update law is given as

$$\dot{\hat{k}}_x = \dot{\hat{k}}_r = 0. \tag{15}$$

While in the instant state, $\hat{k}_x, \hat{k}_r$ are transient at each t_k to complete one step of adaptive update. The adaptation law at the instant t_k is expressed as

$$\hat{k}_x^+ = \hat{k}_x - \frac{\tau_1 x^{\mathrm{T}} P B_m}{a_1 + \|P\|\,\|x\|} - \sigma_1 \hat{k}_x, \hat{k}_r^+ = \hat{k}_r - \frac{\tau_2 x^{\mathrm{T}} P B_m}{a_2 + \|P\|\,\|x\|} - \sigma_2 \hat{k}_r, \tag{16}$$

where $a_1 > 0, a_2 > 0$ are small positive constants, τ_1, τ_2 are the positive adaptive gains, σ_1, σ_2 are the modification term gains, satisfying $0 < \sigma_j < \frac{1}{2}, j = 1, 2$. Define parameter estimation error $\tilde{k}_x = k_x^* - \hat{k}_x, \tilde{k}_r = k_r^* - \hat{k}_r$, the full-time adaptive law is obtained as:

$$\begin{aligned} \dot{\tilde{k}}_x &= 0, t \in [t_k, t_{k+1}), \tilde{k}_x^+ = \tilde{k}_x + \frac{\tau_1 x^{\mathrm{T}} P B_m}{a_1 + \|P\|\,\|x\|} + \sigma_1 \hat{k}_x, t = t_k, \\ \dot{\tilde{k}}_r &= 0, t \in [t_k, t_{k+1}), \tilde{k}_r^+ = \tilde{k}_r + \frac{\tau_2 x^{\mathrm{T}} P B_m}{a_2 + \|P\|\,\|x\|} + \sigma_2 \hat{k}_r, t = t_k. \end{aligned} \tag{17}$$

According to the above adaptive law (17), plant (5) and controller (12), the closed-loop stability analysis is carried out in the next subsection.

Remark 3.1: Note that the excitation condition persists on the reference input r, that is, the regression term $\varphi(\tilde{x}, r)$ also satisfies the Persistent Excitation (PE) condition. Considering the existence of disturbance $\bar{d}_0$ in plant (5), according to **Assumption 2.1**, $\bar{d}_0$ can be denoted as

$$\left\|\bar{d}_0\right\| \leq L_0^* + L^* \|\tilde{x}\| + L_1^* \|\tilde{x}\|^{1+\eta} + L_2^* \|\tilde{x}\|^{1+\theta}, \tag{18}$$

where $L_0^*, L^*, L_1^*, L_2^* \in \mathbb{R}_+$ is considered to be known. Note that due to the power term of the convergence error, it means that the general linear control method cannot suppress this part of the disturbance, which further illustrates the necessity of the nonlinear anti-disturbance controller design.

3.3. Stability Analysis

To analyze the system stability, the following theorem is formulated:

Theorem 3.1: In the drag-free system (5) based on an ETRMRAC scheme, when the input disturbances satisfy (18), there exists $0 < X^{\mathrm{T}} = X \in \mathbb{R}^{n\times n}, Y_j \in \mathbb{R}^{1\times n}, \Phi = \mathrm{diag}\{\phi_i\} > 0$ and $\Omega_j = \mathrm{diag}\left\{\omega_{ji}\right\} > 0, i = 1, ..., n, j = 0, 1, 2$, so that the following linear matrix inequalities:

$$\begin{aligned} & 1_n^{\mathrm{T}}\left[\delta\left(B_m Y_0 + X A_m^{\mathrm{T}}\right) + \chi\left({B_m}^{-1} Y_0 + X A_m^{\mathrm{T}}\right) + \Omega_0\right] \leq 0, \\ & 1_n^{\mathrm{T}}\begin{bmatrix} (1+\eta)\,\delta\left(B_m Y_1 + X A_m^{\mathrm{T}}\right) + (1+\eta)\,\Omega \\ + \eta\chi\left(B_m Y_1 + X A_m^{\mathrm{T}}\right) + \chi^{\mathrm{T}}\left(B_m Y_1 + X A_m^{\mathrm{T}}\right) \end{bmatrix} \leq 0, \\ & 1_n^{\mathrm{T}}\begin{bmatrix} (1+\theta)\,\delta\left(B_m Y_2 + X A_m^{\mathrm{T}}\right) + (1+\theta)\,\Omega \\ + \theta\chi\left(B_m Y_2 + X A_m^{\mathrm{T}}\right) + \chi^{\mathrm{T}}\left(B_m Y_2 + X A_m^{\mathrm{T}}\right) \end{bmatrix} \leq 0, \\ & \Phi > \mu L I_n, 2\Omega_s - \mu L_s L_n > 0, s = 1, 2, \tilde{Q} \leq 0 \end{aligned} \tag{19}$$

holds, where for a fixed $0 < \Lambda_j = \mathrm{diag}\left\{\lambda_{ji}\right\}$,

$$\tilde{Q} = \begin{bmatrix} A_m X + X A_m^{\mathrm{T}} + \Phi + 6 & 0 & 0 & 0 & B_m \\ * & B_m Y_0 + Y_0^{\mathrm{T}} B_m^{\mathrm{T}} + \frac{\mu L_0^*}{n}\Lambda_0^{-2} + 6\Psi_0 & B_m Y_1 + Y_0^{\mathrm{T}} B_m^{\mathrm{T}} & B_m Y_2 + Y_0^{\mathrm{T}} B_m^{\mathrm{T}} & B_m \\ * & * & B_m Y_1 + Y_1^{\mathrm{T}} B_m^{\mathrm{T}} + 6\Psi_1 & B_m Y_2 + Y_1^{\mathrm{T}} B_m^{\mathrm{T}} & B_m \\ * & * & * & B_m Y_2 + Y_2^{\mathrm{T}} B_m^{\mathrm{T}} + 6\Psi_2 & B_m \\ * & * & * & * & -\mu I_n \end{bmatrix}, \tag{20}$$

$\mu \in \mathbb{R}_+$, $\Psi_i = \Lambda_{p_i}^{\mathrm{T}}\Lambda_{p_i}$, $\Lambda_{p_i} = P^{-1}\Lambda_i, i = 0, 1, 2$. 1_n^{T} denotes a column vertor of ones with the dimension n, $\chi(M)$ is the matrix calculated by $\chi(M) = |M - \delta(M)|$ and the definition of $\delta(M)$ is given according to (Franco et al., 2021). Choose k_1,$k_2 > 0$, $k_{j+3}^{\mathrm{T}} = Y_j \Lambda_j$, $P = X^{-1}$, after introducing the adaptive law (17), the controller (12) and the ETM

$$\begin{aligned} t_{k+1} = \inf\{ & t > t_k | \iota(\Phi - \mu L)\,\|\tilde{x}(t)\|^2 - 8\gamma\|x(t)\|^2 - \|x(t)\|^4 \\ & - \|\varphi(t)\|^4 - 2\gamma\|\varepsilon_1(t)\|^2 - 2\varpi\|\varepsilon_2(t)\|^2 - 8\varpi\|\varphi(t)\|^2 \\ & - \iota(\Phi - \mu L)\, m_0 \mathrm{e}^{-m_1 t} = 0\}, \end{aligned} \tag{21}$$

all closed-loop signals are guaranteed to be ultimately uniformly bounded (UUB).

Proof: In the stability analysis, the parameter boundedness in the interevent state and instant state will be firstly discussed, and then the feedback gain estimation error will be analyzed. In the interevent state, the following Lyapunov function is given:

$$V_k = V_{k_x} + V_{k_r} = \tilde{k}_x^{\mathrm{T}}\tilde{k}_x + \tilde{k}_r^{\mathrm{T}}\tilde{k}_r, t \in [t_k, t_{k+1}). \tag{22}$$

It is obvious that $\dot{V}_k = 2\tilde{k}_x^{\mathrm{T}}\dot{\tilde{k}}_x + 2\tilde{k}_r^{\mathrm{T}}\dot{\tilde{k}}_r = 0$. Therefore, only the boundedness of the parameters under instant time needs to be considered. At each time instant, due to the system discontinuity, according to the establishing method of the Lyapunov function for discontinuous systems in Lu et al. (2019), a generalized gradient is utilized to establish Lyapunov-like functions $\Delta V_{k_x}, \Delta V_{k_r}$. At each time instant t_k, the boundedness of the state feedback gain $\hat{k}_x$ is firstly analyzed, and ΔV_{k_x} is organized as:

$$\begin{aligned}
\Delta V_{k_x} &= V_{k_x}^{+} - V_{k_x} = \tilde{k}_x^{T+}\tilde{k}_x^{+} - \tilde{k}_x^{\mathrm{T}}\tilde{k}_x \\
&= \left(\tilde{k}_x + \frac{\tau_1 x^{\mathrm{T}} P B_m}{a_1 + \|P\|\,\|x\|} + \sigma_1 \hat{k}_x\right)^{\mathrm{T}}\left(\tilde{k}_x + \frac{\tau_1 x^{\mathrm{T}} P B_m}{a_1 + \|P\|\,\|x\|} + \sigma_1 \hat{k}_x\right) - \tilde{k}_x^{\mathrm{T}}\tilde{k}_x \\
&\le \frac{\tau_1^2\left(x^{\mathrm{T}} P B_m\right)^2}{\left(a_1 + \|P\|\,\|x\|\right)^2} + \sigma_1^2 \hat{k}_x^{\mathrm{T}}\hat{k}_x \\
&\quad + 2\sigma_1 \tilde{k}_x^{\mathrm{T}}\hat{k}_x + \frac{2\tau_1\left|x^{\mathrm{T}} P B_m\right|\left\|\sigma_1 \hat{k}_x^{\mathrm{T}} + \tilde{k}_x^{\mathrm{T}}\right\|}{a_1 + \|P\|\,\|x\|}.
\end{aligned} \tag{23}$$

Note that $0 \le \frac{\left|x^{\mathrm{T}} P B_m\right|}{a_1 + \|P\|\|x\|} \le \|B_m\|$, (23) is further derived as

$$\Delta V_{k_x} \le \tau_1^2 B_m^2 + \sigma_1^2 \hat{k}_x^{\mathrm{T}}\hat{k}_x + 2\sigma_1 \tilde{k}_x^{\mathrm{T}}\hat{k}_x + 2\tau_1 \tilde{k}_x^{\mathrm{T}} + 2\sigma_1\tau_1 \hat{k}_x^{\mathrm{T}}. \tag{24}$$

Utilizing $\tilde{k}_x = k_x^* - \hat{k}_x$, it can be derived that

$$\begin{aligned}
\Delta V_{k_x} &\le \tau_1^2 B_m^2 + \left(2\sigma_1^2 + \sigma_1\right)\left\|k_x^*\right\|^2 + \left(2\sigma_1^2 - \sigma_1\right)\left\|\tilde{k}_x\right\|^2 \\
&\quad + \left(2\sigma_1\tau_1 + 2\tau_1\right)\left\|\tilde{k}_x\right\| + 2\sigma_1\tau_1\left\|k_x^*\right\| \le -\zeta_1\left\|\tilde{k}_x\right\|^2 + \delta_1,
\end{aligned} \tag{25}$$

where $\zeta_1 = \frac{\sigma_1 - 2\sigma_1^2}{2} > 0, \delta_1 = \tau_1^2 + \left(2\sigma_1^2 + \sigma_1\right)\left\|k_x^*\right\|^2 + 2\tau_1\sigma_1\left\|k_x^*\right\| + \frac{2\left(\tau_1 + \sigma_1\tau_1\right)^2}{\sigma_1 - 2\sigma_1^2}$.

Thus, when $\left\|\tilde{k}_x\right\| \ge \sqrt{\frac{2\delta_1}{\zeta_1}}$, $\Delta V_{k_x} < 0$ is satisfied, that is, V_{k_x} is monotonically decreasing within the interval $\left\{\left\|\tilde{k}_x\right\| \ge \sqrt{\frac{2\delta_1}{\zeta_1}}\right\}$. Since $V_{k_x} \ge 0$, the bounded conclusion of V_{k_x} ensures that $\tilde{k}_x$ is bounded, and will eventually converge to a radius of $B_1 = \sqrt{\frac{2\delta_1}{\zeta_1}}$.

Similarly, the bounded conclusion of the reference input feedback gain estimation error $\tilde{k}_r$ can also be obtained. Establish the Lyapunov-like function ΔV_{k_r}. At each time transient t_k, note that $0 \le \frac{\left|x^{\mathrm{T}} P B_m\right|}{a_2 + \|P\|\|x\|} \le \|B_m\|$ and $\tilde{k}_r = k_r^* - \hat{k}_r$, organize ΔV_{k_r} as:

$$\begin{aligned}
\Delta V_{k_x} &= V_{k_x}^{+} - V_{k_x} = \tilde{k}_x^{T+}\tilde{k}_x^{+} - \tilde{k}_x^{\mathrm{T}}\tilde{k}_x \\
&\le \frac{\tau_2^2\left(x^{\mathrm{T}} P B_m\right)^2}{\left(a_2 + \|P\|\,\|x\|\right)^2} + \sigma_2^2 \hat{k}_r^{\mathrm{T}}\hat{k}_r + 2\sigma_2 \tilde{k}_r^{\mathrm{T}}\hat{k}_r + \frac{2\tau_r\left|x^{\mathrm{T}} P B_m\right|\left\|\sigma_r \hat{k}_r^{\mathrm{T}}\tilde{k}_r^{\mathrm{T}}\right\|}{a_2 + \|P\|\,\|x\|} \\
&\le \tau_2^2 B_m^2 + \left(2\sigma_2^2 + \sigma_2\right)\left\|k_r^*\right\|^2 + \left(2\sigma_2^2 - \sigma_2\right)\left\|\tilde{k}_r\right\|^2 \\
&\quad + \left(2\sigma_2\tau_2 + 2\tau_2\right)\left\|\tilde{k}_r\right\| + 2\sigma_2\tau_2\left\|k_r^*\right\| \le -\zeta_2\left\|\tilde{k}_r\right\|^2 + \delta_2,
\end{aligned} \tag{26}$$

where $\zeta_2 = \frac{\sigma_2 - 2\sigma_2^2}{2} > 0, \delta_2 = \tau_2^2 + \left(2\sigma_2^2 + \sigma_2\right)\left\|k_r^*\right\|^2 + 2\tau_2\sigma_2\left\|k_r^*\right\| + \frac{2\left(\tau_2 + \sigma_2\tau_2\right)^2}{\sigma_2 - 2\sigma_2^2}$.

According to (26), it can also be concluded that V_{k_r} is bounded so that $\tilde{k}_r$ is bounded and will eventually converge to a radius of $B_2 = \sqrt{\frac{2\delta_2}{\zeta_2}}$.

Secondly, under the event-triggered mechanism, the state error boundedness is analyzed. In the time sequence $[t_k, t_{k+1})$, the following Lyapunov function is denoted:

$$\begin{aligned}
V &= V_x + V_{k_x} + V_{k_r} \\
&= \tilde{x}^{\mathrm{T}} P \tilde{x} + 2\sum_{j=0}^{2}\sum_{i=1}^{n}\lambda_{ji}\int_0^{x_i} f_{ji}(s)\,ds + \tilde{k}_x^{\mathrm{T}}\tilde{k}_x + \tilde{k}_r^{\mathrm{T}}\tilde{k}_r.
\end{aligned} \tag{27}$$

Note that $\tilde{k}_x^{\mathrm{T}}\tilde{k}_x + \tilde{k}_r^{\mathrm{T}}\tilde{k}_r = 0$ and Lyapunov equation (14), take the first-order differential on both sides of (27):

$$\begin{aligned}
\dot{V} &= -\tilde{x}^{\mathrm{T}} Q \tilde{x} + 2\tilde{x}^{\mathrm{T}} P B_m k_r^{*-1}\left(u_T + \bar{d}_0 - k_x^{*\mathrm{T}} x - k_r^* r\right) \\
&\quad + 2\sum_{j=0}^{2}\left(\tilde{x}^{\mathrm{T}} A_m^{\mathrm{T}} \Lambda_j f_j(\tilde{x}) + \left(u_T + \bar{d}_0 - k_x^{*T} x - k_r^{*T} r\right)^{\mathrm{T}}\right. \\
&\quad \left.\times k_r^{*T} B_m^{\mathrm{T}} \Lambda_j f_j(\tilde{x})\right)
\end{aligned} \tag{28}$$

Substituting the control law (12) into (28), and it is further derived as

$$\begin{aligned}
\dot{V} &= -\tilde{x}^{\mathrm{T}} Q \tilde{x} + 2\tilde{x}^{\mathrm{T}} P B_m k_r^{*-1}(\hat{k}_x^{\mathrm{T}} x(t_k)\alpha(t_k) - k_x^{*\mathrm{T}} x \\
&\quad + \hat{k}_r r(t_k)\omega(t_k) - k_r^* r + \hat{k}_r(t_k) f(t_k)\omega(t_k) + \bar{d}_0) \\
&\quad + 2\sum_{j=0}^{2}((\hat{k}_x^{\mathrm{T}} x(t_k)\alpha(t_k) - \left(\hat{k}_x^{\mathrm{T}} + \tilde{k}_x^{\mathrm{T}}\right) x \\
&\quad + \hat{k}_r(t_k) r(t_k)\omega(t_k) - \left(\hat{k}_r + \tilde{k}_r\right) r + \hat{k}_r(t_k) f(t_k)\omega(t_k) \\
&\quad + \bar{d})^{\mathrm{T}} k_r^{*T-1} B_m^{\mathrm{T}} \Lambda_j f_j + \tilde{x}^{\mathrm{T}} A_m^{\mathrm{T}} \Lambda_j f_j) \\
&\le -\tilde{x}^{\mathrm{T}} Q \tilde{x} + 2\sum_{j=0}^{2}\tilde{x}^{\mathrm{T}} A_m^{\mathrm{T}} \Lambda_j f_j + 2\left(\tilde{x}^{\mathrm{T}} P + f^{\mathrm{T}}(\tilde{x})\Lambda\right) \\
&\quad \times B_m k_r^{*-1}(\hat{k}_x^{\mathrm{T}} x(t_k)\alpha(t_k) - \hat{k}_x^{\mathrm{T}} x + \hat{k}_r(t_k)\varphi(t_k)\omega(t_k) \\
&\quad - \hat{k}_r\varphi + k_r^* f + \bar{d}) + 2\left(\|\tilde{x}\|\,\|P\| + \|f(\tilde{x})\|\,\|\Lambda\|\right) \\
&\quad \times \|B_m\|\left\|k_r^{*-1}\right\|\left(\|\tilde{k}_x^{\mathrm{T}} x\| + \|\tilde{k}_r\varphi\|\right).
\end{aligned} \tag{29}$$

Some items in (29) are analyzed separately:

$$\begin{aligned}
&2\left(\tilde{x}^{\mathrm{T}} P + f^{\mathrm{T}}(\tilde{x})\Lambda\right) B_m k_r^{*-1}\left(\hat{k}_x^{\mathrm{T}} x(t_k)\,\alpha(x(t_k)) - \hat{k}_x^{\mathrm{T}} x\right) \\
&= 2\left(\tilde{x}^{\mathrm{T}} P + f^{\mathrm{T}}(\tilde{x})\Lambda\right) B_m k_r^{*-1}\left(-\hat{k}_x^{\mathrm{T}} x + \hat{k}_x^{\mathrm{T}} x(t_k)\right. \\
&\quad \left.\times \tanh\left(\frac{1}{\epsilon}\hat{k}_x^{\mathrm{T}} x(t_k)\left(\tilde{x}^{\mathrm{T}}(t_k) P + f^{\mathrm{T}}(\tilde{x}(t_k))\Lambda\right) B_m\right)\right) \\
&= 2\left(\tilde{x}^{\mathrm{T}} P + f^{\mathrm{T}}(\tilde{x})\Lambda\right) B_m k_r^{*-1}\hat{k}_x^{\mathrm{T}}\left(-x + x\tanh\left(\frac{1}{\epsilon}\right.\right. \\
&\quad \left.\left.\times \hat{k}_x^{\mathrm{T}} x\left(\tilde{x}^{\mathrm{T}} P + f^{\mathrm{T}}(\tilde{x})\Lambda\right) B_m\right)\right) + 2\left(\tilde{x}^{\mathrm{T}} P + f^{\mathrm{T}}(\tilde{x})\Lambda\right) \\
&\quad \times B_m k_r^{*-1}\hat{k}_x^{\mathrm{T}}\left(x(t_k)\tanh\left(\frac{1}{\epsilon}\hat{k}_x^{\mathrm{T}} x(t_k)\left(\tilde{x}^{\mathrm{T}}(t_k) P\right.\right.\right. \\
&\quad \left.\left.\left. + f^{\mathrm{T}}(\tilde{x}(t_k))\Lambda\right) B_m\right) - x\tanh\left(\frac{1}{\epsilon}\hat{k}_x^{\mathrm{T}} x\left(\tilde{x}^{\mathrm{T}} P + f^{\mathrm{T}}(\tilde{x})\Lambda\right) B_m\right)\right).
\end{aligned} \tag{30}$$

According to Wang & Chen. (2020), (30) is further rewritten as:

$$
\begin{aligned}
&2\left(\tilde{x}^{\mathrm{T}}P+f^{\mathrm{T}}(\tilde{x})\Lambda\right)B_m k_r^{*-1}\left(\hat{k}_x^{\mathrm{T}}x(t_k)\,\alpha(x(t_k))-\hat{k}_x^{\mathrm{T}}x\right)\\
&\leq 0.557k_r^{*-1}\epsilon+2\left\|\left(\tilde{x}^{\mathrm{T}}P+f^{\mathrm{T}}(\tilde{x})\Lambda\right)B_m k_r^{*-1}\right\|\left\|\hat{k}_x^{\mathrm{T}}\right\|(\|x\|+\|x(t_k)\|)\\
&\leq 0.557k_r^{*-1}\epsilon+2\left\|\left(\tilde{x}^{\mathrm{T}}P+f^{\mathrm{T}}(\tilde{x})\Lambda\right)B_m k_r^{*-1}\right\|\left\|\hat{k}_x^{\mathrm{T}}\right\|(2\|x\|+\|\varepsilon\|)\\
&\leq 0.557k_r^{*-1}\epsilon+2\|\tilde{x}\|^2+2\left\|P^{-1}f^{\mathrm{T}}(\tilde{x})\Lambda\right\|^2\\
&+2\|B_m\|^2\left\|k_r^{*-1}\right\|^2\|P\|^2\left\|\hat{k}_x^{\mathrm{T}}\right\|^2\left(4\|x\|^2+\|\varepsilon_1\|^2\right),
\end{aligned}
\tag{31}
$$

where, the fact of $|\tanh(\beta/\xi)|\leq 1$ is applied to the derivation. Similarly, it can be obtained that

$$
\begin{aligned}
&2\left(\tilde{x}^{\mathrm{T}}P+f^{\mathrm{T}}(\tilde{x})\Lambda\right)B_m k_r^{*-1}\left(k_r^{\mathrm{T}}\varphi(t_k)\,\omega(x(t_k))-k_r^{\mathrm{T}}\varphi\right)\\
&\leq 0.557k_r^{*-1}\epsilon+2\|\tilde{x}\|^2+2\left\|P^{-1}f^{\mathrm{T}}(\tilde{x})\Lambda\right\|^2\\
&+2\|B_m\|^2\left\|k_r^{*-1}\right\|^2\|P\|^2\left\|\hat{k}_r^{\mathrm{T}}\right\|^2\left(4\|\varphi\|^2+\|\varepsilon_2\|^2\right).
\end{aligned}
\tag{32}
$$

After processing the remaining terms in (29), it can be derived:

$$
\begin{aligned}
&2\left(\tilde{x}^{\mathrm{T}}P+f^{\mathrm{T}}(\tilde{x})\Lambda\right)B_m k_r^{*-1}\tilde{k}_r^{\mathrm{T}}\varphi\\
&\leq\|\tilde{x}\|^2+\left\|P^{-1}f^{\mathrm{T}}(\tilde{x})\Lambda\right\|^2+\|P\|^4\|B_m\|^4\left\|k_r^{*-1}\right\|^4\left\|\tilde{k}_r\right\|^4+\|\varphi\|^4,\\
&2\left(\tilde{x}^{\mathrm{T}}P+f^{\mathrm{T}}(\tilde{x})\Lambda\right)B_m k_r^{*-1}\tilde{k}_x^{\mathrm{T}}x\\
&\leq\|\tilde{x}\|^2+\left\|P^{-1}f^{\mathrm{T}}(\tilde{x})\Lambda\right\|^2+\|P\|^4\|B_m\|^4\left\|k_x^{*-1}\right\|^4\left\|\tilde{k}_x\right\|^4+\|x\|^4.
\end{aligned}
$$

Substituting the above inequalities into (29), it can be further organized as:

$$
\begin{aligned}
\dot{V}\leq&\begin{bmatrix}\tilde{x}\\ f_0\\ f_1\\ f_2\\ \bar{d}_0\end{bmatrix}^{\mathrm{T}}
\begin{bmatrix}
PA_m+A_m^{\mathrm{T}}P+6 & PA_0+A_m^{\mathrm{T}}\Lambda_0 & PA_1+A_m^{\mathrm{T}}\Lambda_1 & PA_2+A_m^{\mathrm{T}}\Lambda_2 & PB_m\\
* & \Lambda_0A_0+A_0^{\mathrm{T}}\Lambda_0+\dfrac{\mu L_0^*}{n}I_n+6\Psi_0 & \Lambda_1A_1+A_0^{\mathrm{T}}\Lambda_0 & \Lambda_2A_2+A_0^{\mathrm{T}}\Lambda_0 & B_m^{\mathrm{T}}\Lambda_0\\
* & * & \Lambda_1A_1+A_1^{\mathrm{T}}\Lambda_1+6\Psi_1 & \Lambda_2A_2+A_1^{\mathrm{T}}\Lambda_1 & B_m^{\mathrm{T}}\Lambda_1\\
* & * & * & \Lambda_2A_2+A_2^{\mathrm{T}}\Lambda_2+6\Psi_2 & B_m^{\mathrm{T}}\Lambda_2\\
* & * & * & * & -\mu
\end{bmatrix}
\begin{bmatrix}\tilde{x}\\ f_0\\ f_1\\ f_2\\ \bar{d}_0\end{bmatrix}\\
&-\frac{\mu L_0^*}{n}f_0^{\mathrm{T}}f_0+\mu\bar{d}_0^{\mathrm{T}}\bar{d}_0+\bar{W}+\|x\|^4+\|\varphi(\tilde{x},r)\|^4\\
&+8\gamma\|x\|^2+8\varpi\|\varphi(\tilde{x},r)\|^2+2\gamma\|\varepsilon_1\|^2+2\varpi\|\varepsilon_2\|^2,
\end{aligned}
\tag{33}
$$

where, $\Psi_j=P^{T-1}P^{-1}\Lambda_j\Lambda_j^{\mathrm{T}}$, $j=0,1,2$, $A_0=B_mk_3$, $A_1=B_mk_4$, $A_2=B_mk_5$, $\gamma=\|B_m\|^2\left\|\bar{k}_r^{*-1}\right\|^2\|P\|^2\left\|\hat{k}_x^{\mathrm{T}}\right\|^2$, $\varpi=\|B_m\|^2\left\|k_r^{*-1}\right\|^2\|P\|^2\left\|\hat{k}_r\right\|^2$, $\bar{W}=\sup_{t\in[0,+\infty)}\{W\}$, $W=\|P\|^4\|B_m\|^4\left\|k_x^{*-1}\right\|^4\times\left\|\tilde{k}_x\right\|^4+\|P\|^4\|B_m\|^4\left\|k_r^{*-1}\right\|^4\left\|\tilde{k}_r\right\|^4+1.114\left\|k_r^{*-1}\right\|\epsilon$. Then $\dot{V}$ can be denoted as

$$
\begin{aligned}
\dot{V}=&\,\xi^{\mathrm{T}}Q_b\xi-\frac{\mu L_0^*}{n}f_0^{\mathrm{T}}f_0+\mu\bar{d}_0^{\mathrm{T}}\bar{d}_0+\|x\|^4+\|\varphi(\tilde{x},r)\|^4\\
&+\bar{W}+2\gamma\|x\|^2+2\varpi\|\varphi(\tilde{x},r)\|^2+2\gamma\|\varepsilon_1\|^2+2\varpi\|\varepsilon_2\|^2,
\end{aligned}
\tag{34}
$$

where

$$
Q_b=\begin{bmatrix}
A_mX+XA_m^{\mathrm{T}}+6P^{-2} & B_mY_0+XA_m^{\mathrm{T}} & B_mY_1+XA_m^{\mathrm{T}} & B_mY_2+XA_m^{\mathrm{T}} & B_m\\
* & B_mY_0+Y_0^{\mathrm{T}}B_m^{\mathrm{T}}+\dfrac{\mu L_0^*}{n}\Lambda_0^{-2}+6\Psi_0\Lambda_0^{-2} & B_mY_1+Y_0^{\mathrm{T}}B_m^{\mathrm{T}} & B_mY_2+Y_0^{\mathrm{T}}B_m^{\mathrm{T}} & B_m\\
* & * & B_mY_1+Y_1^{\mathrm{T}}B_m^{\mathrm{T}}+6\Psi_1\Lambda_0^{-2} & B_mY_2+Y_1^{\mathrm{T}}B_m^{\mathrm{T}} & B_m\\
* & * & * & B_mY_2+Y_2^{\mathrm{T}}B_m^{\mathrm{T}}+6\Psi_2\Lambda_0^{-2} & B_m\\
* & * & * & * & -\mu
\end{bmatrix}.
\tag{35}
$$

To ensure that Q_b is semi-negative definite, some items in the matrix

$$
\begin{aligned}
Q_{b12}&=Q_{b21}=B_mY_0+XA_m^{\mathrm{T}},\\
Q_{b13}&=Q_{b31}=B_mY_1+XA_m^{\mathrm{T}},\\
Q_{b14}&=Q_{b41}=B_mY_2+XA_m^{\mathrm{T}},
\end{aligned}
\tag{36}
$$

and their symmetric counterparts are processed as in Ge & Tao. (2021). Taking these terms out of Q_b, then (33) can be expressed as

$$
\begin{aligned}
\dot{V}=&\,\xi^{\mathrm{T}}\tilde{Q}\xi-\tilde{x}^{\mathrm{T}}\Phi\tilde{x}-2\sum_{j=0}^{2}\tilde{x}^{\mathrm{T}}\Omega_jf_j(\tilde{x})-\frac{\mu L_0^*}{n}f_0^{\mathrm{T}}f_0\\
&+2\sum_{j=0}^{2}\tilde{x}^{\mathrm{T}}\left(B_mY_j+XA_m^{\mathrm{T}}+\Omega_j\right)f_j(\tilde{x})+\mu\bar{d}_0^{\mathrm{T}}\bar{d}+\|x\|^4\\
&+\|\varphi(\tilde{x},r)\|^4+\bar{W}+8\gamma\|x\|^2+8\varpi\|\varphi(\tilde{x},r)\|^2\\
&+2\gamma\|\varepsilon_1\|^2+2\varpi\|\varepsilon_2\|^2,
\end{aligned}
\tag{37}
$$

where the form of $\tilde{Q}$ has been given by (20). Therefore, to guarantee the stability of the system, it is necessary to select the main diagonal elements of $B_mY_j+XA_m^{\mathrm{T}}+\Omega_j$ to be semi-negative definite. Then the above-mentioned matrix cross terms can be processed according to Wang et al. (2022):

$$
\begin{aligned}
\tilde{x}_if_0(\tilde{x}_k)&\leq|\tilde{x}_i|,\\
\tilde{x}_if_1(\tilde{x}_k)&\leq\frac{|\tilde{x}_i|^{1+\eta}}{1+\eta}+\frac{\alpha|\tilde{x}_i|^{1+\eta}}{1+\eta},\\
\tilde{x}_if_2(\tilde{x}_k)&\leq\frac{|\tilde{x}_i|^{1+\theta}}{1+\theta}+\frac{\gamma|\tilde{x}_i|^{1+\theta}}{1+\theta},
\end{aligned}
\tag{38}
$$

where $i\neq k$. Take Q_{b13} as an example to analyze the upper bound of $B_mY_j+XA_m^{\mathrm{T}}+\Omega_j$, it is obtained by applying the above inequalities:

$$
\begin{aligned}
&1_n^{\mathrm{T}}\delta(Q_{b13})|\tilde{x}|^{\eta+1}+1_n^{\mathrm{T}}\frac{\eta\chi(Q_{b13})}{1+\eta}|\tilde{x}|^{\eta+1}\\
&+1_n^{\mathrm{T}}\frac{\chi^{\mathrm{T}}(Q_{b13})}{1+\eta}|\tilde{x}|^{\eta+1}+1_n^{\mathrm{T}}\Omega_1|\tilde{x}|^{\eta+1}\leq 0.
\end{aligned}
\tag{39}
$$

Utilizing the LMIs availability in (19) and (20) to analyze the above equation, the corresponding

$\tilde{x}^{\mathrm{T}}\left(B_m Y_j + X A_m^{\mathrm{T}} + \Omega_j\right) f_j(\tilde{x}) \le 0$ can be obtained. Thus, the upper bound of $\dot{V}$ is expressed as:

$$\begin{aligned}\dot{V} \le & -\tilde{x}^{\mathrm{T}}\Phi\tilde{x} - 2\sum_{j=0}^{2}\tilde{x}^{\mathrm{T}}\Omega_j f_j(\tilde{x}) - \frac{\mu L_0^*}{n} f_0^{\mathrm{T}} f_0 + \mu \bar{d}_0^{\mathrm{T}}\bar{d} \\ & + \|x\|^4 + \|\varphi(\tilde{x},r)\|^4 + \bar{W} + 8\gamma\|x\|^2 + 8\varpi\|\varphi(\tilde{x},r)\|^2 \\ & + 2\gamma\|\varepsilon_1\|^2 + 2\varpi\|\varepsilon_2\|^2.\end{aligned} \tag{40}$$

According to **Assumption 2.1**, it is further derived that

$$\begin{aligned}\dot{V} = & -\tilde{x}^{\mathrm{T}}(\Phi - \mu L)\tilde{x} - \sum_{s=1}^{2}\tilde{x}^{\mathrm{T}}\left(2\Omega_j - \mu L_s\right) f_s(\tilde{x}) \\ & + \|x\|^4 + \bar{W} - 2\tilde{x}^{\mathrm{T}}\Omega_0 f_0(\tilde{x}) + \|\varphi(\tilde{x},r)\|^4 \\ & + 8\gamma\|x\|^2 + 8\varpi\|\varphi(\tilde{x},r)\|^2 + 2\gamma\|\varepsilon_1\|^2 + 2\varpi\|\varepsilon_2\|^2.\end{aligned} \tag{41}$$

Substituting the ETM (21), further analysis is expressed as:

$$\begin{aligned}\dot{V} = & -\tilde{x}^{\mathrm{T}}(\Phi - \mu L)(1-\iota)\tilde{x} + \bar{W} + (\Phi - \mu L)\iota m_0 \mathrm{e}^{-m_1 t} \\ & - \sum_{s=1}^{2}\tilde{x}^{\mathrm{T}}\left(2\Omega_j - \mu L_s\right) f_s(\tilde{x}) - 2\tilde{x}^{\mathrm{T}}\Omega_0 f_0(\tilde{x}),\end{aligned} \tag{42}$$

where $0 < \iota < 1$. Correct the designed Lyapunov function as:

$$V_r = V + \frac{(\Phi - \mu L)\iota}{m_1} m_0 \mathrm{e}^{-m_1 t}. \tag{43}$$

Then the first-order differential of V_r in each interevent state $[t_k, t_{k+1})$ satisfies

$$\begin{aligned}\dot{V}_r = & \tilde{x}^{\mathrm{T}}(\Phi - \mu L)(1-\iota)\tilde{x} + \bar{W} \\ & - \sum_{s=1}^{2}\tilde{x}^{\mathrm{T}}\left(2\Omega_j - \mu L_s\right) f_s(\tilde{x}) - 2\tilde{x}^{\mathrm{T}}\Omega_0 f_0(\tilde{x}).\end{aligned} \tag{44}$$

That is, there is always an interval of $\|\tilde{x}\| \ge W^*$, such that $\dot{V}_r \le 0$. When considering triggering time, note that $V_r^+ - V_r = V_{k_x}^+ + V_{k_r}^+ - V_{k_x} - V_{k_r}$, system state does not change. Combining (25) and (26), it can be concluded that when $\|\tilde{x}\| \ge W^*$, $\left\|\tilde{k}_x\right\| \ge B_1, \left\|\tilde{k}_r\right\| \ge B_2$, V_r monotonically decreases. Thus it can be proved that, under the arbitrarily selected initial value, the global closed-loop signals can achieve stable tracking to the reference model and are guaranteed to be ultimately uniformly bounded (UUB), the system state converges to a set around the origin.

3.4. Feasibility Analysis

The feasibility analysis is shown to exclude the Zeno behavior, which presents the phenomenon of infinite triggering in a finite time interval. Assume that Zeno behavior occurs at t_k, then it is extended that $\lim\limits_{k\to+\infty} t_k = T_0$, with the constant $T_0 \in \mathbb{R}_+$. That is,

$$t_k \in [T_0 - \varepsilon_0, T_0], \forall k \ge N_0, \tag{45}$$

where $N_0 \in \mathbb{N}_+$, $\varepsilon_0 \in \mathbb{R}_+$, which is selected as

$$\varepsilon_0 = \frac{1}{2\|A_m\|}\ln\left(\frac{\|A_m\|}{\Theta}\left(\sqrt{m_0}\mathrm{e}^{-\frac{1}{2}m_1 T_0} - C\right) + 1\right) > 0, \tag{46}$$

where Θ, C is defined later in this subsection. Recalling (11) and calculating the derivation of $\|\tilde{x}\|$ as:

$$\begin{aligned}\left\|\dot{\tilde{x}}\right\| = & \|A_m\tilde{x} + B_m k_r^{*-1}(u_T - k_x^* x - k_r^*\varphi(\tilde{x},r) \\ & + k_r^*\left(\bar{d}_0 + K^{\mathrm{T}} f(\tilde{x})\right))\| \\ \le & \|A_m\|\,\|\tilde{x}\| + B_m k_r^{*-1}(u_T - k_x^* x - k_r^*\varphi(\tilde{x},r) \\ & + k_r^*\left(\bar{d}_0 + K^{\mathrm{T}} f(\tilde{x})\right)) \\ \le & \|A_m\|\,\|\tilde{x}\| + \Theta,\end{aligned} \tag{47}$$

where $\Theta \in \mathbb{R}_+$, $\|B_m\|\left\|k_r^{*-1}\right\|(\|u_T\| - \left\|k_x^*\right\|\|x\| - \left\|k_r^*\right\|\|\varphi(x,r)\| + \left\|k_r^*\right\|\left\|\bar{d}_0 + K^{\mathrm{T}} f(\tilde{x})\right\|) \le \Theta$ holds during $t \in [0,\infty)$. Define $\|\tilde{x}(t_k)\| = c$, according to the lemma given in Wang et al. (2018), for $t \in [t_k, t_{k+1})$, $\|\tilde{x}\|$ is derived as

$$\|\tilde{x}\| \le \frac{\Theta}{\|A_m\|}\left[\mathrm{e}^{\|A_m\|(t-t_k)} - 1\right] + c. \tag{48}$$

It can be obtained that $\lim\limits_{t\to\infty}\sup\|c\| \le C$ from the boundedness of $\tilde{x}$, and $t_{k+1} - t_k$ can represent the evolution time for $\|\tilde{x}\|$ from c^2 to $\iota(\Phi - \mu L)\|\tilde{x}\|^2 - 8\gamma\|x\|^2 - \|x\|^4 - \|\varphi(\tilde{x},r)\|^4 - 8\varpi\|\varphi(\tilde{x},r)\|^2 - \iota(\Phi - \mu L)m_0\mathrm{e}^{-m_1 t}$. Thus, the lower bound τ_k of $t_{k+1} - t_k$ can be obtained by the following equation:

$$\frac{\Theta}{\|A_m\|}\left[\mathrm{e}^{\|A_m\|(t-t_k)} - 1\right] = \sqrt{m_0}\mathrm{e}^{-\frac{1}{2}m_1 T_0} - C. \tag{49}$$

From selecting the suitable parameters, it can be guaranteed $\sqrt{m_0}\mathrm{e}^{-\frac{1}{2}m_1 T_0} - C$, $\tau_k = 2\varepsilon_0$ can be obtained, and $t_{k+1} \ge t_k + \tau_k \ge T_0 + \varepsilon_0$ can also be found. The derivation above contradicts the hypothesis (44), thus Zeno behavior is excluded.

4. Simulation Results and Analysis

Numerical simulation verification is presented based on the sample drag-free control nonlinear dynamic system (Fichter et al., 2007). In the simulation, the closed-loop performance of the ETRMRAC scheme for displacement noise suppression in 2-DOFs of the sensitive axis is shown, and the triggering interval under the ETM is compared with the time triggering mechanism (TTM) (Basu et al., 2017). For the general TTM, the controller is derived as a continuous-time form, while in the simulation verification, the control input is updated with a fixed sampling step, and the updating frequency is set to be 10Hz according to Fichter et al. (2007); Basu et al. (2017). According to Wu & Fertin. (2008), for the dynamic modeling of the drag-free control system, the stiffness matrix with perturbation is set as

$$\begin{aligned}&{\Omega_{DF}}^2 = 10^{-7} \times (1 \pm 10\%) \\ &\times \begin{bmatrix} 11.19 & 1.35 & 1.35 & 0.00425 & 0 & 0 \\ 1.35 & 9.55 & 1.35 & 0.00425 & 0 & 0 \\ 1.35 & 1.35 & 24.12 & 0.00425 & 0 & 0 \\ 26.087 & 26.087 & 26.087 & 30.64 & 0 & 0 \\ 0 & 0 & 0 & 0 & 9.55 & 1.35 \\ 0 & 0 & 0 & 0 & 1.35 & 24.12 \end{bmatrix},\end{aligned}$$

and the input matrix is set as

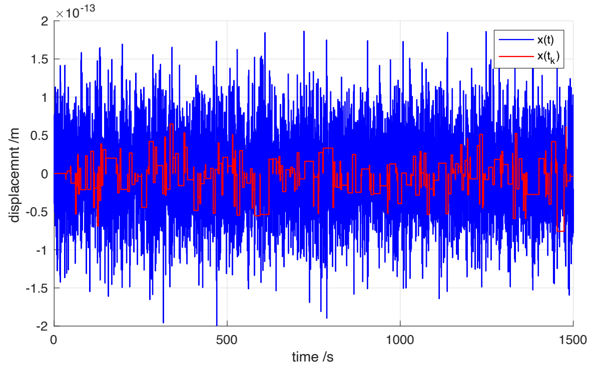

Fig. 3. Comparison of time-triggered response and interevent response under ETM in x_1 axis.

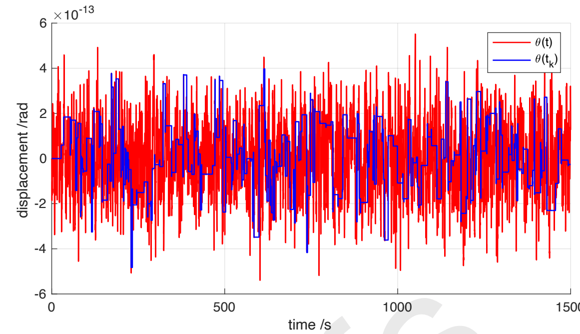

Fig. 4. Comparison of time-triggered response and interevent response under ETM in θ_2 axis.

$$B_{DF} = \begin{bmatrix} -1 & 0 & 0 & 0 & 0 & 0 \\ 0 & -1 & 0 & 0.45 & 0 & 0 \\ 0 & 0 & -1 & 0 & 0 & 0 \\ 0 & 0 & 0 & -1 & 0 & 0 \\ 0 & 0 & 0 & 0 & -1 & 0 \\ 0 & 0 & 0 & 0 & 0 & -1 \end{bmatrix}.$$

The control parameter are choosen as $\eta = 0.89, \theta = 1.12, \tau_1 = \tau_2 = \mathrm{diag}(1000, 500, 1000, 5000), \sigma_1 = \sigma_2 = 0.2, Q = \mathrm{diag}(8 \times 10^{-7}, 8 \times 10^{-7}, 8 \times 10^{-7}, 8 \times 10^{-7}), A_m = \mathrm{diag}(8 \times 10^{-4}, 8 \times 10^{-4}, 8 \times 10^{-4}, 8 \times 10^{-4}), m_0 = 1 \times 10^{-56}, m_1 = 0.4$. The bounded disturbances are given in Mobley et al. (1975). Simulation continues 1500 s, and the sample step under TTM is set to 0.1 s. Simulation results are shown in Fig. 3 to Fig. 15.

Fig. 3 and Fig. 4 show the comparison of state feedback for input signals before and after being triggered by the ETM. The ETM has a certain reduction effect on the control amplitude when dealing with high-frequency bounded disturbances. In the control signal comparison shown in Fig. 5 and Fig. 6, the average amplitude of the control signal under ETM is smaller than TTM, which is effective for the realization of the low cost of actuator energy. In Fig. 7 and Fig. 8, the comparison of closed-loop signal state responses based on two different mechanisms shows that the closed-loop signal disturbance suppression effect under time triggered controller is stronger than that of an event-triggered controller, but the displacement noise under event-triggered control scheme is still within the performance requirements of the sample mission of space gravitational wave detection. Fig. 9 and Fig. 10 show the comparison of the triggering time interval under the ETM and the triggering times of the TTM. Under a total of 15,000 sampling steps, the ETM only triggers 456 times to ensure the stability of the closed-loop system and a reasonable closed-loop control effect, which intuitively reflects the superiority of ETM for the triggering numbers.

Fig. 11 and Fig. 12 show the control performance comparison between the ETRMRAC scheme and the time-triggered control scheme (Wu & Fertin., 2008) with QFT for displacement disturbance suppression. The simulation results show that in the detection frequency band, although the event-triggered scheme does not update the control input all the time, due to the strong nonlinear uncertainty suppression ability and additional

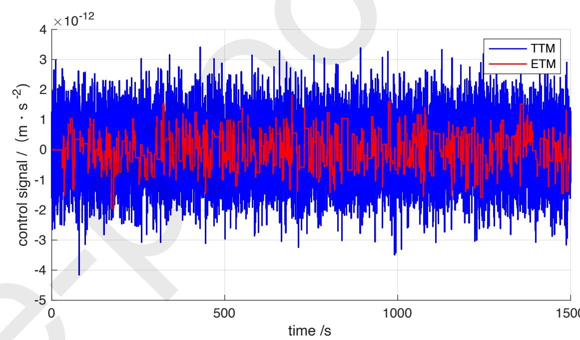

Fig. 5. Comparison of control signal under ETM and TTM in x_1 axis.

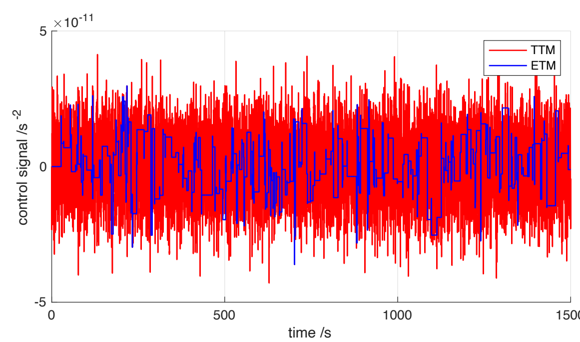

Fig. 6. Comparison of control signal under ETM and TTM in θ_2 axis.

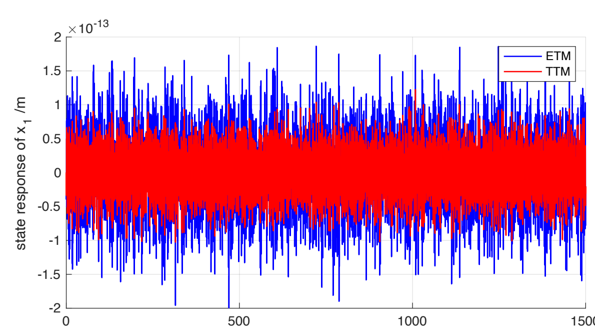

Fig. 7. Comparison of state response under ETM and TTM in x_1 axis.

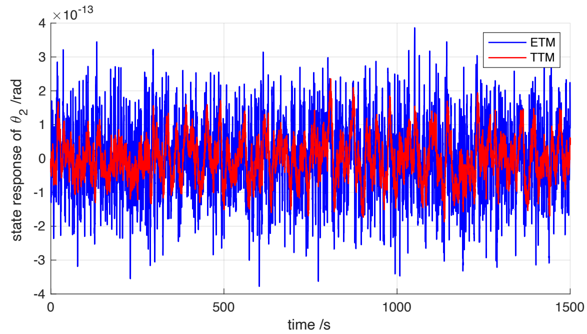

Fig. 8. Comparison of state response under ETM and TTM in θ_2 axis.

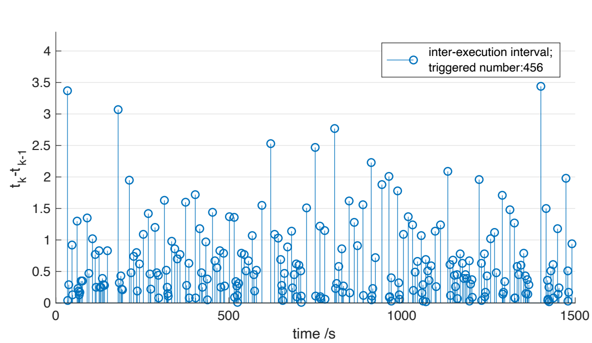

Fig. 9. Trigger transient and time interval under ETM.

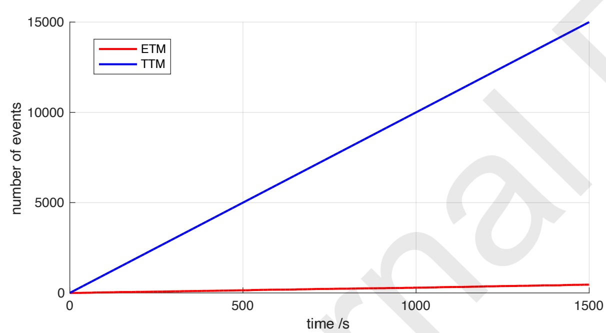

Fig. 10. Comparison of trigger times under ETM and TTM.

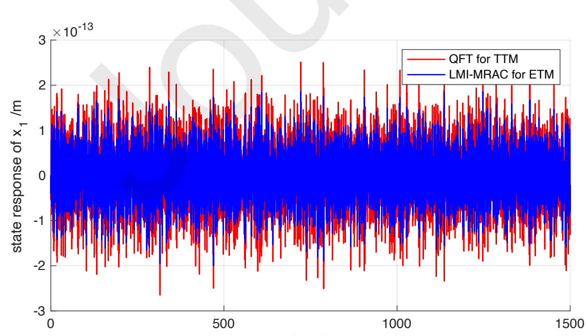

Fig. 11. Comparison of state response under various scheme in x_1 axis.

robustness, under the presence of continuous high-frequency nonlinear disturbances, it still provides better control performance than the QFT scheme.

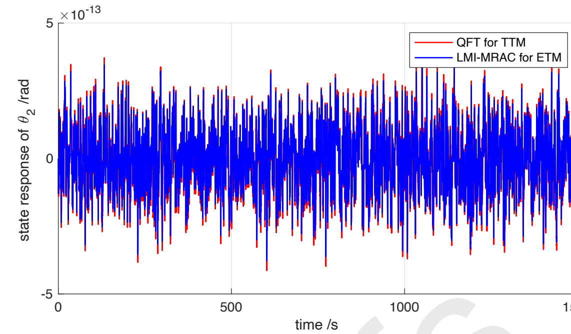

Fig. 12. Comparison of state response under various scheme in θ_2 axis.

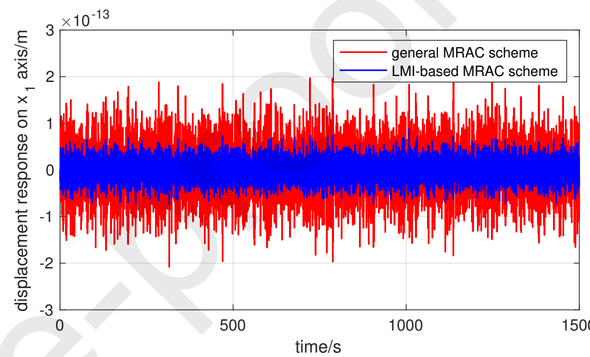

Fig. 13. Comparison of state response with parameter perturbation under general MRAC and LMI-based MRAC in x_1 axis.

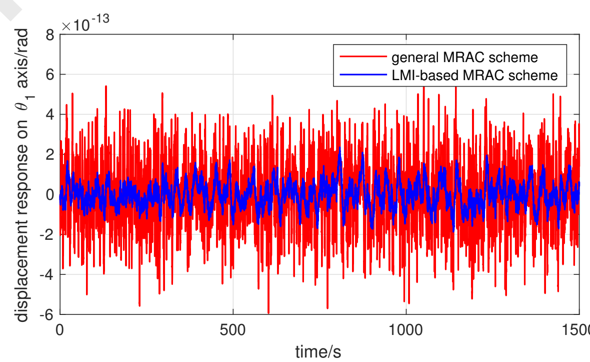

Fig. 14. Comparison of state response with parameter perturbation under general MRAC and LMI-based MRAC in θ_2 axis.

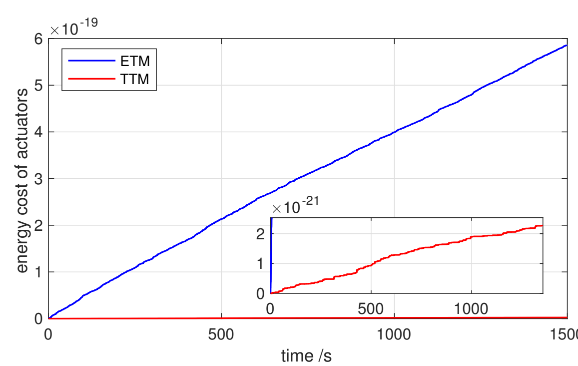

Fig. 15. Comparison of energy cost of actuators under ETM and TTM.

Fig. 13 and Fig. 14 show the comparison of state responses on the simulated axes, between the proposed LMI-based MRAC scheme and general adaptive control scheme (Ahmadi et al., 2020) under the time-triggering mechanism. The simulation results show that under the 10% perturbation of the stiffness matrix, the LMI-based MRAC scheme can perform more efficient anti-disturbance ability than the general MRAC scheme, which clarified the effectiveness of the proposed LMI-based robust compensator.

Fig. 15 shows the control energy consumption reduction of the proposed event-triggered mechanism, to reflect the saving of controller information burden, since the control input remains constant during the triggering interval, which does not require energy to drive the actuators and does not exchange any information. We utilize the following energy calculation method to implement the comparison:

$$E = \sum_{t=0}^{T} \Delta u_T^T(t)\, \Delta u_T(t)$$

where $=u_T(t) - u_T(t-t_0)$ denotes the derivative of $u_T(t)$, t_0 is the sampling step. According to the simulation results, the energy consumption of the TTM case is much higher than the cost of the ETM case, which verifies the control energy consumption reduction of the proposed event-triggered mechanism. Combined with Fig. 10, it can be concluded that the saving of controller information burden achieves through the TTM approach.

5. Conclusion

In this paper, a novel event-triggered MRAC scheme based on the LMI approach is designed, which is applied for the drag-free control problem in the mission of low-frequency space gravitational wave detection, to reduce the communication burden and realize the low cost of the actuator energies, with the Zeno behavior being strictly excluded. In the event-triggered MRAC scheme, an LMI approach is introduced, which enhances the system stability margin compared with the general control scheme (Basu et al., 2017) while ensuring the tracking performance. The Lyapunov analysis proves the ultimate boundedness of each closed-loop signal, and the numerical simulation verifies the good control performance of the event-triggered robust MRAC scheme.

Acknowledgments

This work is supported in part by National Key Research and Development Program of the Ministry of Science and Technology of China under Grant 2020YFC2200800, National Natural Science Foundation of China under Grant 62103275 and General project of Shanghai Natural Science Foundation under Grant 20ZR1427000.

References

Ahmadi, K., Pazooki, F., & Roshanian, J. (2020). Model reference adaptive control of a small satellite in the presence of parameter uncertainties. *Scientia Iranica*, (pp. 2933–2944).

Basu, R. S., Bhasin, S., & Kar., I. (2017). Combined mrac for unknown mimo lti systems with parameter convergence. *IEEE Transactions on Automatic Control.*, *63*(1), 283–290.

Enrico., C. (2008). Drag-free and attitude control for the goce satellite. *Automatica.*, *44*(7), 1766–1780.

Enrico, C., Molano, A., & Massotti., L. (2009). Drag-free control of the goce satellite: noise and observer design. *IEEE Transactions on Control Systems Technology.*, *18*(2), 501–509.

Fichter, W., Gath, P., Vitale, S. et al. (2005). Lisa pathfinder drag-free control and system implications. *Classical and Quantum Gravity.*, *22*(10), S139.

Fichter, W., Schleicher, A., Bennani, S. et al. (2007). Closed loop performance and limitations of the lisa pathfinder drag-free control system. In *in AIAA Guidance, Navigation and Control Conference and Exhibit.* (p. 6732).

Franco, R., Rios, H., de Loza, A. F. et al. (2021). A robust nonlinear model reference adaptive control for disturbed linear systems: An lmi approach. *IEEE Transactions on Automatic Control.*, .

Ge, S., & Tao., G. (2021). Partial-state feedback multivariable mrac and reduced-order designs. *Automatica.*, *129*, 109622.

Grynagier, A., Ziegler, T., & Fichter., W. (2013). Identification of dynamic parameters for a one-axis drag-free gradiometer. *IEEE Transactions on Aerospace and Electronic Systems.*, *49*(1), 341–355.

Gui., H. (2021). Observer-based fault-tolerant spacecraft attitude tracking using sequential lyapunov analyses. *IEEE Transactions on Automatic Control.*, .

Li, B., Hu, Q., Ma, G. et al. (2019). Fault-tolerant attitude stabilization incorporating closed-loop control allocation under actuator failure. *IEEE Transactions on Aerospace and Electronic Systems.*, *55*(4), 1989–2000.

Li, B., Hu, Q., Yu, Y. et al. (2017). Observer-based fault-tolerant attitude control for rigid spacecraft. *IEEE Transactions on Aerospace and Electronic Systems.*, *53*(5), 2572–2582.

Lian, X., & et al. (2021). Frequency separation control for drag free satellite with frequency domain constraints. *IEEE Transactions on Aerospace and Electronic Systems.*, *57*(6), 4085–4096.

Liang, H., & et al. (2020). Neural-network-based event-triggered adaptive control of nonaffine nonlinear multiagent systems with dynamic uncertainties. *IEEE Transactions on Neural Networks and Learning Systems.*, *32*(5), 2239–2250.

Liu, W., Geng, Y., Wu, B. et al. (2020). Neural-network-based adaptive event-triggered control for spacecraft attitude tracking. *IEEE Transactions on Neural Networks and Learning Systems.*, *31*(10), 4015–4024.

Long, L., & Wang., F. (2021). Dynamic event-triggered adaptive nn control for switched uncertain nonlinear systems. *IEEE Transactions on Cybernetics.*, .

Lu, M., Liu, L., & Feng, G. (2019). Adaptive tracking control of uncertain euler–lagrange systems subject to external disturbances. *Automatica.*, *104*, 207–219.

Luisella, G., Fenal, T., & Wu., S. (2013). Attitude and orbit control systems for the lisa pathfinder mission. *Aerospace Science and Technology.*, *24*(1), 283–294.

McNamara, P., & et al. (2008). Lisa pathfinder. *Classical and quantum gravity.*, *25*(11), 114034.

Mobley, F., Fountain, G., Sadilek, A. et al. (1975). Electromagnetic suspension for the tip-ii satellite. *IEEE Transactions on Magnetics.*, *11*(6), 1712–1716.

Qian, Y. Y., Liu, L., & Feng., G. (2021). Cooperative output regulation of linear multiagent systems: An event-triggered adaptive distributed observer approach. *IEEE Transactions on Automatic Control.*, *66*(2), 833–840.

Qiu, J., Sun, K., Wang, T. et al. (2019). Observer-based fuzzy adaptive event-triggered control for pure-feedback nonlinear systems with prescribed performance. *IEEE Transactions on Fuzzy Systems.*, *27*(11), 2152–2162.

Shen, Q., & et al. (2020). Fault modeling, estimation, and fault-tolerant steering logic design for single-gimbal control moment gyro. *IEEE Transactions on Control Systems Technology.*, *29*(1), 428–435.

Shen, Q., Yue, C., Goh, C. et al. (2018). Active fault-tolerant control system design for spacecraft attitude maneuvers with actuator saturation and faults. *IEEE Transactions on Industrial Electronics.*, *66*(5), 3763–3772.

Wang, A., Liu, L., Qiu, J. et al. (2018). Event-triggered robust adaptive fuzzy control for a class of nonlinear systems. *IEEE Transactions on Fuzzy Systems.*, *27*(8), 1648–1658.

Wang, A., Liu, L., Qiu, J. et al. (2022). Event-triggered adaptive fuzzy output-feedback control for nonstrict-feedback nonlinear systems with asymmetric output constraint. *IEEE Transactions on Cybernetics.*, *52*(1), 712–722.

Wang, L., & Chen., C. P. (2020). Reduced-order observer-based dynamic event-triggered adaptive nn control for stochastic nonlinear systems subject to unknown input saturation. *IEEE Transactions on Neural Networks and Learning Systems.*, *32*(4), 1678–1690.

Wu, S., & et al. (2010). Attitude control of lisa pathfinder spacecraft with micro-newton feep thrusters under multiple failures. In *in AIAA Guidance, Navigation and Control Conference.*.

Wu, S., & et al. (2011). Attitude stabilization of lisa pathfinder spacecraft using colloidal micro-newton thrusters. In *in AIAA Guidance, Navigation and Control Conference.*.

Wu, S., & Fertin., D. (2008). Spacecraft drag-free attitude control system design with quantitative feedback theory. *Acta Astronautica.*, *62*(12), 668–682.

Xing, L., & et al. (2016). Event-triggered adaptive control for a class of uncertain nonlinear systems. *IEEE Transactions on Automatic Control.*, *62*(4), 2071–2076.

Zanoni, C., & Bortoluzzi., D. (2015). Experimental-analytical qualification of a piezoelectric mechanism for a critical space application. *IEEE/ASME Transactions on Mechatronics.*, *20*(1), 427–437.

Zhang, C. H., & Yang., G. H. (2018). Event-triggered adaptive output feedback control for a class of uncertain nonlinear systems with actuator failures. *IEEE Transactions on Cybernetics.*, *50*(1), 201–210.

Zhang, H., & et al. (2021). Event-triggered adaptive tracking control for random systems with coexisting parametric uncertainties and severe nonlinearities. *IEEE Transactions on Automatic Control.*, .

Ziegler, T., Bergner, P., Hechenblaikner, G. et al. (2014). Modeling and performance of contact-free discharge systems for space inertial sensors. *IEEE Transactions on Aerospace and Electronic Systems.*, *50*(2), 1493–1510.

Declaration of interests

☒ The authors declare that they have no known competing financial interests or personal relationships that could have appeared to influence the work reported in this paper.

☐The authors declare the following financial interests/personal relationships which may be considered as potential competing interests: